Measurements of the Rates of the Decay $\pi^+ \rightarrow \pi^0 + e^+ + \nu$ and of π^- Capture in LiH, CH_2, and CH†

D. BARTLETT, S. DEVONS, S. L. MEYER,* AND J. L. ROSEN
Columbia University, New York, New York
(Received 1 July 1964)

We have measured the branching ratio for $\pi^+ \rightarrow \pi^0 + e^+ + \nu$. Our method exploited the near anticollinearity of the two γ rays resulting from the subsequent decay of the π^0. The detection of these γ rays using spark chambers, together with the identification of the positron in a scintillation target detector, enabled us to identify the pion beta-decay process in a manner which was effectively free from background. On the basis of 39 events, of which 3 are attributed to background, and an independent calibration of the over-all efficiency of the apparatus, we deduce for the branching ratio $(0.97\pm0.020)\times10^{-8}$, in agreement with previous measurements and the prediction of the conserved-vector-current hypothesis. Using the same apparatus, we have also measured W, the fraction of stopped π^- mesons captured by hydrogen nuclei bound in chemical compounds. We find $W_{\mathrm{LiH}}=(40\pm4)\times10^{-3}$, $W_{\mathrm{CH_2}}=(17.9\pm1.9)\times10^{-3}$, and $W_{\mathrm{CH}}=(5.5\pm0.7)\times10^{-3}$. Negative pion capture in H_2-N_2 and H_2-He gas mixtures has also been briefly studied.

I. INTRODUCTION

THE remarkably close agreement between the vector coupling constant $G_V{}^\beta$, derived from nuclear beta-decay measurements, and that obtained from $\mu-e$ decay poses a question. Why are the vector coupling constants for muons and nucleons so closely equal? Why is the vector coupling constant apparently unmodified by the strong interactions? The analogy with electromagnetic currents, where electric charge is unchanged by the strong interactions, has led to the formulation of a general conservation law for vector-coupled weak interactions: the conserved-vector-current hypothesis (CVC).[1,2]

This hypothesis leads to additional relationships between corresponding electromagnetic and weak interactions and specific predictions about the latter. Several tests of these have already been made. The modification of the B^{12}, N^{12} spectra, predicted by Gell-Mann,[3] has been measured[4,5] to confirm the CVC hypothesis. The explicit introduction of a pion current leads directly to another prediction of CVC, namely that the branching ratio for pion beta decay is[6]

$$R=\frac{\mathrm{rate}(\pi^+\rightarrow\pi^0+e^+\nu)}{\mathrm{rate}(\pi^+\rightarrow\mu^+\nu)}\underset{\mathrm{CVC}}{=}(1.03\pm0.03)\times10^{-8}. \quad (1)$$

Despite the experimental difficulties involved in measuring such a small branching ratio, other experiments using techniques different from ours have indeed confirmed the CVC prediction to within 20%.[7,8] Our experiment, which we shall describe in detail in the following sections, is of the same accuracy and is consistent with these measurements.

II. EXPERIMENT

A. Basic Technique

The accuracy with which this small branching ratio can be measured is limited by two factors: first, the obvious statistical limitation owing to the paucity of events; second, the difficulty in isolating unambiguously true events from a severe background. The main emphasis in our experiment has been on eliminating the latter source of error.

The separation of the events from the background is greatly aided by the distinctive features of the pion beta decay. When the π^+ decays from rest, the maximum velocity of the emitted π^0 is only 0.03 c, and consequently, the angle between the γ rays from the π^0 decay is between 176.4 and 180°. Spark chambers having good spatial resolution were used to distinguish these nearly anticollinear γ rays from background γ rays. Some of these may arise from decays of neutral pions produced in charge exchange reactions. These pairs of γ rays will cover a much wider range of angles. Other background γ rays may be totally uncorrelated. Moreover, associated with each genuine pair of γ rays, there is simultaneously the positron of the beta decay. These positrons were detected since the π^+ mesons were stopped in a plastic scintillator. A typical event contained a double pulse: a large pusle produced by the stopping π^+ and a small pulse due to the positron in beta decay. Our over-all criterion was to observe two anticollinear γ rays in coincidence with a decay positron, but delayed with respect to the stopping π^+ (mean life 25.5 nsec).

† Work supported in part by the U. S. Office of Naval Research.
* Present address: Rutgers, The State University, New Brunswick, New Jersey.
[1] S. Gershtein and Ya. B. Zel'dovich, Zh. Eksperim. i Teor. Fiz. **29**, 698 (1955) [English transl.: Soviet Phys.—JETP **2**, 576 (1957)].
[2] R. Feynman and M. Gell-Mann, Phys. Rev. **109**, 193 (1958).
[3] M. Gell-Mann, Phys. Rev. **111**, 362 (1958).
[4] T. Mayer-Kuckuk and F. C. Michel, Phys. Rev. **127**, 545 (1962).
[5] Y. K. Lee, L. W. Mo, and C. S. Wu, Phys. Rev. Letters **10**, 253 (1963).
[6] M. V. Terent'ev, Zh. Eksperim. i Teor. Fiz. **44**, 1320 (1963) [English transl.: Soviet Phys.—JETP **17**, 890 (1963)].
[7] P. Depommier, J. Heintze, C. Rubbia, and V. Soergel, Phys. Letters **5**, 61 (1963).
[8] A. F. Dunajtsev, V. I. Petrukhin, Yu. D. Prokoshkin, and V. I. Rykalin, Joint Institute for Nuclear Research, Dubna, 1964 (to be published).

Good detection efficiency was achieved by surrounding the scintillator target as completely as possible with steel-plate spark chambers. The details of the construction of these is discussed in Sec. II C below.

B. Beam and Electron Detectors

A positive pion beam of mean momentum $\sim$145 MeV/c was extracted from the cyclotron, and subsequently momentum analyzed, focused, and moderated so that the stopping distribution peaked at the center of the $1\frac{1}{2}$-in. thick target counter. Using the general arrangement shown in Fig. 1, it was possible to stop 50 000 π/sec, with a duty cycle of 30%, in the target scintillation counter (7-in. diam).

In order to measure the opening angle between the gammas, it is necessary to know the location of the stopping pion. This information comes from two sources. An aluminum-foil spark chamber placed immediately in front of the target counter permitted the reconstruction of the two coordinates which are perpendicular to the beam axis. A measure of the depth of penetration of the pion into the target counter was provided by the size of the stopping pion pulse.

The target counter was designed to provide both good energy and timing resolution. The pion pulse height could be used to determine the depth of the stopping to within $\frac{1}{4}$ in. The positron (of 2-MeV average energy) could be distinguished from the tail of the stopping pion pulse (about 20 MeV) when the positron came as soon as 10 nsec after the stopping. The Naton 136 scintillator plastic was viewed by a 58 AVP photomultiplier, operated with a low over-all voltage and a low-impedance voltage supply to the last stages to preserve the linearity of the response for stopping pion pulses.

Figure 2 shows schematically the arrangement of the beam telescope and of the gamma detectors described in the next section.

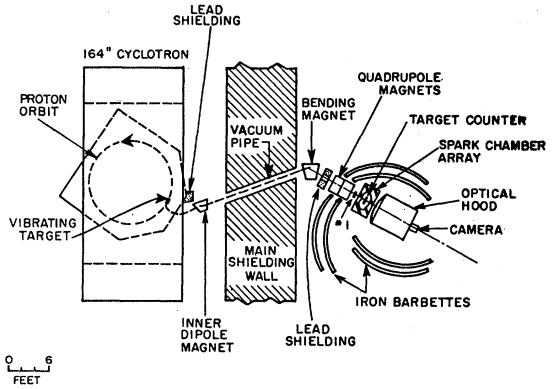

FIG. 1. Geometry of the beam and general layout of the detecting apparatus.

C. Detector: Spark-Chamber Array and Optics

The target scintillation counter in which the pions were stopped was surrounded on four sides by interleaved spark chambers and counters. The spark chambers were of modular construction and, in all, twelve were used in the array. One of the four identical sides is indicated in Fig. 3. Each side consisted of three spark-chamber modules stacked in the direction normal to the beam with scintillation counters between each module and the next. An additional inside layer of scintillation counters constituted an anticoincidence shield against charged particles entering the stack. The counters following each spark-chamber module comprised the "gamma counters" and detected the electrons resulting from the conversion of gammas in the stainless-steel plates of the spark chambers. The gamma

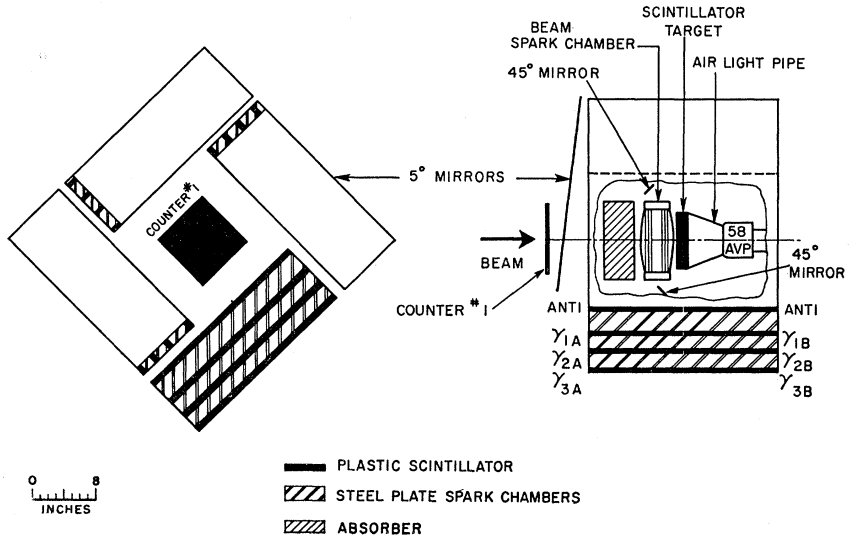

FIG. 2. Schematic diagram of the apparatus. (For clarity, drawing shows apparatus with one 5° mirror removed.)

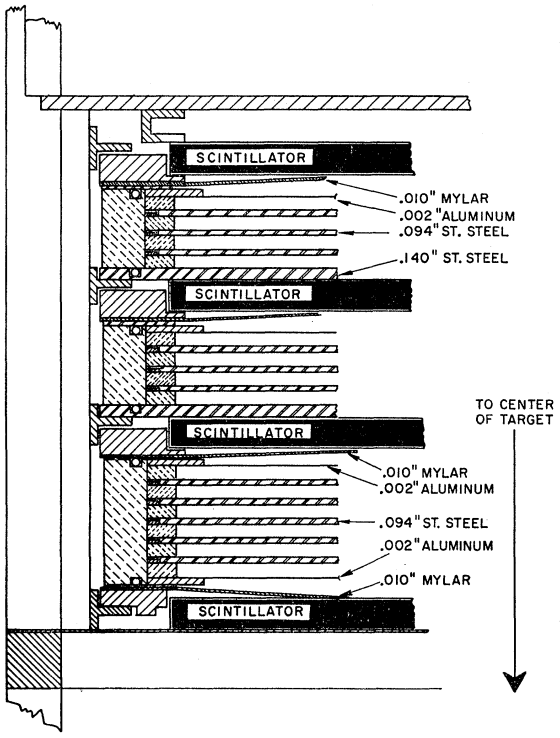

FIG. 3. Details of construction of a bank of γ chambers. Total thickness of steel is 1.31 in. $\approx$ 1.9 radiation lengths $\approx$ 1.1 conversion lengths for 67.5-MeV γ's.

detection efficiency of this "sandwich" array will be discussed in more detail in Sec. IV.

The eight inner counters making up the anticoincidence shield and the twenty-four gamma counters used to detect the conversion electrons were of identical construction: Each was a $24\times12\times\frac{1}{2}$-in. scintillation plastic sheet viewed through the 12-in. edge by one RCA 6655A photomultiplier. Despite their large dimensions, the variation in pulse height across a typical counter was less than 30%, and the timing uncertainty was about 6 nsec.

The optical system used to view the spark chambers was severely constrained by the geometry of the array, which made it impractical to view each chamber from more than one side. As shown in Fig. 4, the chambers were photographed with a single camera through a 36-in.-square cut spherical lens of 15-ft focal length. The use of back mirrors effectively yielded 10° stereo. Each spark gave two images on the film: one coming directly from the spark and the other coming from the spark's reflection in a mirror rotated by 5° away from the beam side of the spark chambers. The distance between the photographed images of the spark and its reflection is proportional to the distance between the spark and the 5° mirror, and hence is a measure of the depth of the spark in the chamber. The accuracy with which the depth coordinate could be measured was $\frac{1}{4}$ in. This is comparable to the uncertainty in determining the stopping plane of the pion in the target counter.

D. Electronic Logic and Recording

The isolation of the rare pion beta-decay process was accomplished in two rather conventional steps. First, "logic" elements such as coincidence circuits were used to define the electronic conditions which pion beta decays were expected to satisfy. Second, when these conditions were fulfilled, a "trigger" was provided to spark chambers and oscilloscopes in which the details of the process were displayed, and to a camera drive circuit which advanced the two 35-mm cameras used to view the oscilloscopes and the spark chamber array. The pictures taken were subsequently analyzed and approximately one event which satisfied all the criteria for a pion beta decay was found for every 3000 triggers.

The basic triggering requirement was that two γ rays be observed in coincidence at any time between 8 and 70 nsec after the passage of a beam particle (π^+). The triggering requirement itself imposed moderately stringent anticollinearity requirements on the γ rays. The gammas were required not only to go to opposite banks of detectors but also to the downstream counter stack of one bank and the upstream stack of the other; e.g., the coincidence $1A$-$3B$ was an acceptable trigger but $1A$-$3A$ was not. The outputs of the three gamma counters of a given stack were mixed and coincidences between stacks formed in the manner indicated in Fig. 5.

A fast coincidence between a gamma counter and a beam particle vetoed the trigger and reduced the background due to charge exchange in flight

$$\pi^+ + C \rightarrow N^* + \pi^0,$$

which is a prompt process. A further reduction in false triggers was made by eliminating, electronically, decay

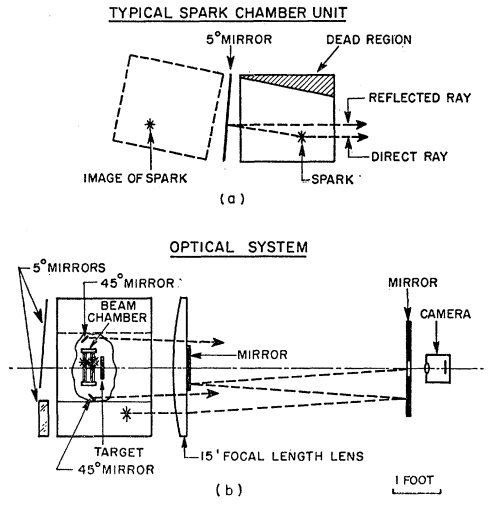

FIG. 4. Diagram of optics. Figure 4(a) shows method of obtaining 10° stereo view. Figure 4(b) shows system used to photograph spark chambers.

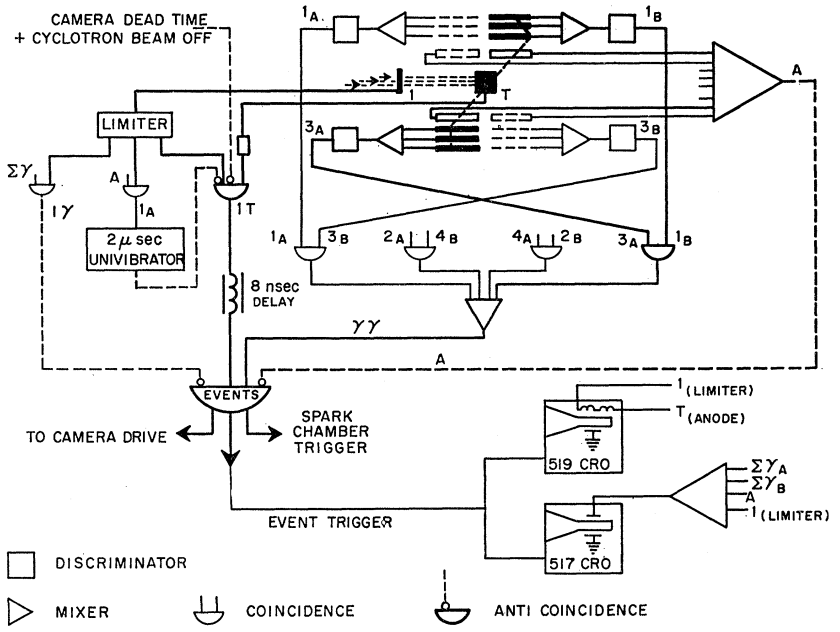

FIG. 5. Block diagram of the electronic logic. The heavy lines indicate the main requirements imposed for a typical event.

electrons coming from pions which had been scattered and stopped in the gamma spark chambers. A (1-A) coincidence generated a 2-μsec gate which was put in anticoincidence with the event trigger.

The event trigger had two functions. One output went to a hard-tube spark-gap pulser which fired five spark gaps, one for each bank of gamma spark chambers and one for the beam spark chamber. A second output triggered two fast Tektronix oscilloscopes, a 517A and a 519. The 519, a traveling-wave oscilloscope, was used to display the pulse from the target scintillation counter and the amplitude-limited pulse from No. 1 (the first beam counter). On the 40-nsec/cm sweep, it was possible to distinguish the positron pulse on the tail of the stopping pion pulse and also to measure the time interval between the two pulses. The 20-nsec/cm sweep of the 517A was used to display a pulse $\sum\gamma_A$ consisting of the twelve mixed upstream gamma counters, a pulse $\sum\gamma_B$ constituting the twelve mixed downstream gamma counters, and also the beam (No. 1) pulse to permit the times of the positron and the gammas to be compared for candidate events. As a precaution against electronic failure, the pulses from the eight anticounters were mixed and displayed. This pulse would have appeared only if an anticounter had given a pulse which failed to operate the appropriate anticoincidence circuit.

E. Operation

The pion beta-decay experiment involved approximately 20 days during which events were recorded. During this time, 0.78×10^{11} pions were stopped and 125 000 pictures were taken. Frequent checks of the stability of the beam and the equipment were made. In addition to the beam and trigger rates, the T-A (decay electron), 1-A (scattered pion), and 1-γ rates were continuously monitored. These rates were recorded and compared every two hours to check for drifts in the electronics.

The 32 gamma counters and anticounters were timed with a nanosecond light pulser, and their gains adjusted by means of cosmic rays several times during the 20 days. No significant drifts were found.

Finally, at the end of the run, the calibration and the experiment involving negative-pion absorption in hydrogenous materials were made. These are described in Sec. VI and VII, respectively.

III. SCANNING AND DATA ANALYSIS

A. Isolating the Events

Despite our efforts to reduce the background before triggering, 90% of the pictures taken showed either no sparks or no recognizable pattern. Table I outlines the selection criteria which were applied to the remaining pictures.

The requirement that there be a single-beam (No. 1) pulse was imposed to remove accidental coincidences

TABLE I. Selection criteria.

Criterion	Number of pictures surviving
Two tracks, each comprising two or more contiguous sparks, in opposite chambers	10 000
Single-beam (No. 1) pulse	5000
Positron pulse within 25 nsec of γ time	1000
Opening angle of event in the direct view greater than 165°	486

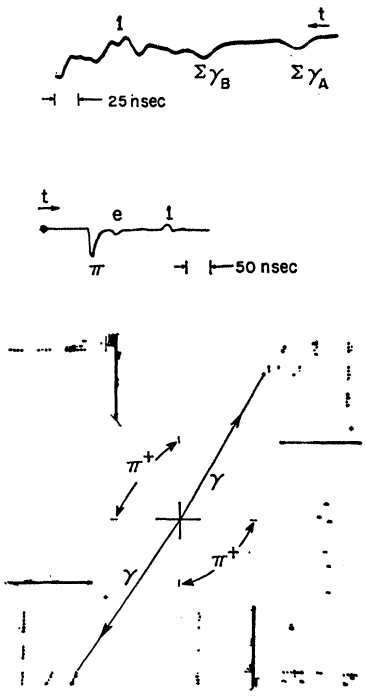

FIG. 6. Oscilloscope and spark-chamber patterns for a typical event. The spark-chamber pattern also shows fiducial lights and their reflections and slight edge sparks which could easily be identified. On the top trace, the ripples following the $\Sigma\gamma_B$ pulse are caused by the firing of the spark chambers.

between charge-exchange gammas and an earlier beam particle.

The 486 selected candidates were measured and their characteristics punched on IBM cards. From the spark-chamber film, a record was made of the coordinates of the beam particle and both conversion points and of the number of gaps firing in both γ-ray showers. From the oscilloscope film, measurements were made of the time and height of the π, e, and No. 1 pulses (519 oscilloscope) and of the $\sum\gamma_A$, $\sum\gamma_B$, and No. 1 pulses (517 oscilloscope). The width of the No. 1 pulse on the 519 was also noted, since anomalously wide No. 1 pulses were caused by two particles passing through the No. 1. counter in quick succession. A typical pattern for a pion beta-decay event is shown in Fig. 6.

We then required that the No. 1 pulse have a width compatible with that of a single particle and that the π-e time equal the 1-γ time to within 10 nsec. The effect of these and other requirements in reducing the background is summarized in Table II.

All four γ-γ triggering modes contributed approximately equally to the remaining 82 pictures. These were remeasured and differences (5 cases) resolved. Finally, to remove background, identifiable as such when the total energy released in the γ-ray showers is small, it was demanded that the total number of gaps firing in both sides be greater than six. This requirement reduced the total number of candidates to 69. Of these, we shall show that 36 are examples of pion beta decay and the remainder are background. In order to show how this separation is achieved, however, we must first consider the reconstruction of the opening angle between the two γ rays.

TABLE II. Summary of number of candidates eliminated by various criteria.

Criterion	Total
No elimination	468
Edge sparks in depth dimension	−85
No. 1 width >28 nsec	−130
Extra pulses	−21
Two γ rays more than 10 nsec mistimed (γ—No. 1) time more than 10 nsec	−9
different from (e—π) time	−135
e height greater than 20 MeV	−3
(γ—No. 1) time within 10 nsec of prompt time	−3
	82
Total gaps firing ≤ 6	−13
	69
Background in scatter plot	−30
Events	39

B. Reconstructing the Opening Angle

The only necessary coordinate not determined directly from the spark-chamber pictures is the depth to which the π^+ penetrated the $1\frac{1}{2}$-in.-thick target counter before stopping. This coordinate is determined to within about $\frac{1}{4}$ in. by the following procedure. Using the integral range curve, the target counter is divided into five "regions" in each of which an equal number of pions have stopped. Similarly, from a histogram of pion pulse heights, the stopping pion pulses could be sorted into five groups containing equal numbers. By pairing these two groups of five, an event having a given pulse height was assigned a depth given by the center line of the corresponding region.

The resulting resolution in the depth angle ($\approx 4°$) was still much worse than the resolution in the projected angle ($\approx \frac{1}{2}°$), which could be measured directly.

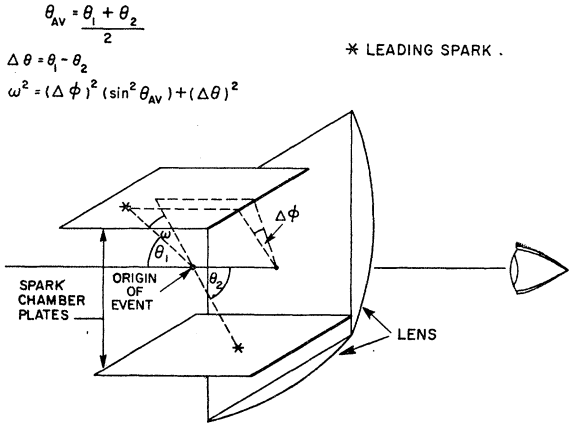

FIG. 7. Definition of angles between the γ rays. These angles are used in scatter plot of events (Fig. 8).

Consequently, in presenting the results, it is desirable to give a scatter plot of events using these two angles as axes rather than to give a simple histogram of events versus opening angle. Furthermore, the scatter plot is easy to understand if the angles between one gamma ray and the *reversed* direction of the other gamma ray are used. In this way, an exactly anticollinear event lies at the origin of the scatter plot and small-angle formulas become immediately obvious. Figure 7 gives a precise definition of the depth angle ($\Delta\theta$) and the projected angle ($\Delta\phi$). We note that for small opening angles ω

$$\omega^2 = (\Delta\phi)^2 \sin^2\theta_{av} + (\Delta\theta^2). \quad (2)$$

A scatter plot of the 69 candidates using $|\Delta\theta|$ and $|\Delta\phi \sin\theta_{av}|$ as axes is given in Fig. 8.

C. Background Subtraction

Figure 8 shows a pronounced cluster of 39 events near the origin. However, some background subtraction is needed. From Eq. (2) and our choice of axes, it is evident that an *isotropic* background would yield a *uniform* density of points. If we *assume* the background is isotropic in the region of opening angle less than 20°, and make small corrections for loss of sensitivity at the larger opening angles, then the extrapolated background is 3 ± 1 events. We wish to emphasize that in order to make this subtraction, we need not know the specific nature of the background, but need only assume that it is isotropic.

We have, however, estimated the contribution of various possible sources of background. The most dangerous of these is radiative e decay of the pion, $\pi^+ \rightarrow e^+ + \nu + \gamma$ (with subsequent external e^+ bremsstrahlung). Pion structure-dependent effects suggest that the e^+-γ angular correlation for this process has a secondary maximum at 180°. Thus, if the radiative decay of the pion were responsible for most of the background, the assumption of linear extrapolation would be questioned. However, using the recent

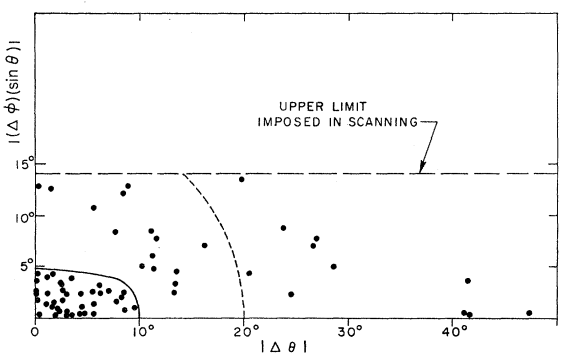

FIG. 8. Scatter plot of the 69 candidates showing 39 events within the solid curve. The background obtained by extrapolating the density of points in the region bounded by the dashed curve is 3 ± 1.

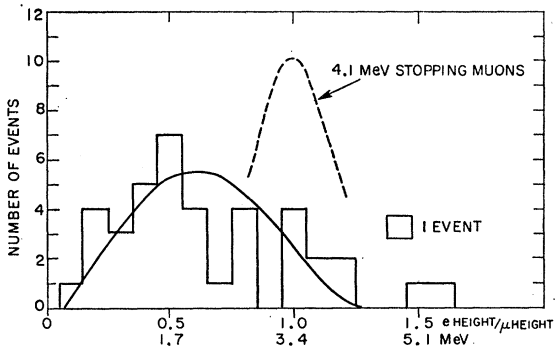

FIG. 9. Histrogram of positron heights for the 39 events. The theoretical spectrum has been raised by 0.25 MeV to allow for the average energy given by positron annihilation radiation. There were no events in which the positron had an energy greater than 6 MeV.

measurements of Depommier *et al.*,[9] and the theoretical angular correlations of Bludman and Young,[10] we expect that the radiative decay of the pion will only contribute 0.7 ± 0.3 events, and that the density of this background in the event region of the scatter plot is only 1.5 times as high as that of the contiguous region. Thus, we may safely conclude that consideration of the radiative pion decay affects only negligibly our assumption of an isotropic background.

A radiative muon decay, $\mu^+ \rightarrow e^+ + \nu + \nu^- + \gamma$, can also simulate an event if the muon pulse is hidden in the pion pulse and the positron radiates. The angular distribution for this process is quite flat for e^+-γ opening angles between 160 and 180°. Using the theoretical transition rates for the emission of electrons and gamma rays of various energies as given and checked experimentally by Parker, Anderson, and Rey,[11] we estimate that the background from radiative muon decay is 0.8 ± 0.4 events.

D. Electron Spectrum and Time Distribution

The distribution of positron pulse heights for the 39 events is shown in Fig. 9. This distribution agrees with the expected positron spectrum for an allowed beta-decay transition having an end point of 4.1 MeV. The theoretical spectrum has been shifted by 0.25 MeV along the x axis to allow for the average energy given by positron annihilation radiation within the target. The energy scale was calibrated with stopping muons. Using the curves of Wright,[12] we find that, owing to saturation effects in the scintillator, a pulse from a 4.13-MeV stopping muon is equal to a 3.4-MeV positron pulse.

[9] P. Depommier, J. Heintze, C. Rubbia, and V. Soergel, Phys. Letters **7**, 285 (1963).
[10] Sidney A. Bludman and James A. Young, Phys. Rev. **118**, 602 (1960).
[11] Sherwood Parker, Herbert L. Anderson, and Charles Rey, Phys. Rev. **133**, B768 (1964).
[12] G. T. Wright, Phys. Rev. **91**, 1282 (1953).

Figure 10 shows the distribution of events versus the time between the pion and positron pulses. Shown on the same curve is the expected pion lifetime (25.5 nsec) normalized to all counts obtained after 15 nsec. The agreement is seen to be good; the lifetime determined from the events themselves is 25±4 nsec.

IV. THE EFFICIENCY

The efficiency is essentially the product of two factors: the probability that the positron pulse will be discernible and within the delayed gate, and the probability that both gamma rays will be converted and detected.

A. Efficiency for Detecting the Positron

The positron detection efficiency was determined empirically using the observed π-μ decays. We triggered the oscilloscope on beam particles (1-T) at a low beam rate and observed that 656 out of 1377 traces have visible muons falling within the delayed gate. Thus, the probability per 1-T trigger of seeing a muon is just $656/1377=0.48\pm0.014$. The probability of seeing a pion beta-decay positron is, of course, somewhat less since the positron spectrum extends down to zero energies. Events in which there was less than a 1-mm deflection would not be detected. Such a deflection corresponds to about 0.7-MeV total energy or about 0.5-MeV positron energy. The probability of a pion-decay positron having an energy less than 0.5 MeV is 4%. Thus we have for the positron detection efficiency

$$P((e)/(1\text{-}T))=0.46\pm0.02.$$

We wish to emphasize that this detection efficiency is normalized to *beam particles*, not stopping pions. This normalization is reasonable since the directly measured rate is the (1-T) rate. However, as a check on our method of extracting the efficiency, we computed the ratio of stopping pions to beam particles by fitting an exponential to the plot of π-μ times for the 656 muons, computing the number of parent pions and comparing this number with the number of (1-T) triggers (see Fig. 11). This computation yields

$$\frac{\text{stopping pions}}{(1-T)}=\frac{1100}{1377}=0.80\pm0.03,$$

in good agreement with the ratio of 0.76 obtained from the integral range curve.

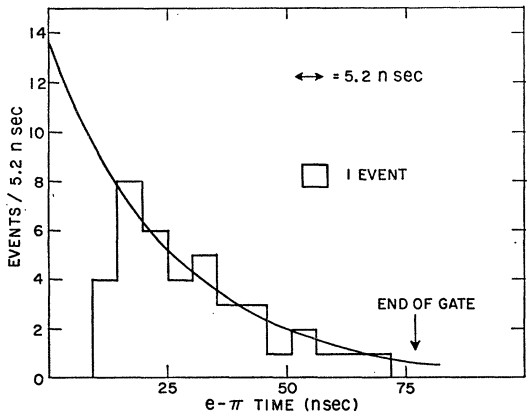

FIG. 10. Histogram of positron-pion times. The smooth curve is an exponential having the present value of the mean pion life (25.5 nsec) normalized to all counts after 15 nsec.

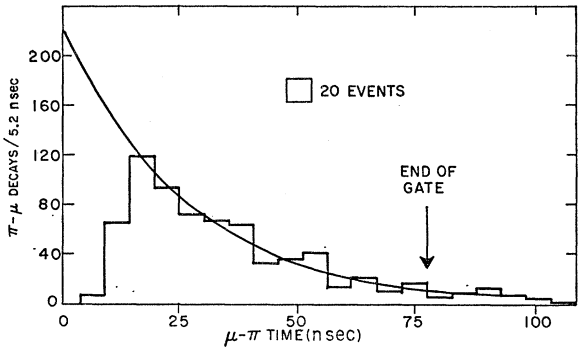

FIG. 11. Histogram of muon-pion times for ≈700 $\pi\rightarrow\mu$ decays. The exponential is fitted by the least-squares method to all events having times greater than 15 nsec and yields a mean life of (26.0±1.0) nsec.

B. Gamma-Ray Detection Efficiency

It is necessary to determine the probability that a gamma ray incident on a bank of spark chambers and counters will be converted and detected. This problem was solved by using the Monte Carlo technique of Butcher and Messel[13] to simulate electron-photon showers. The Monte Carlo program determined the probability that in a shower induced by a 67.5-MeV photon there would be one or more electrons at any of depths $d/3$, $2d/3$, or d. The calculation was "one-dimensional," i.e., scattering was neglected. However, we insured that the calculation would correspond reasonably with the physical situation by choosing one parameter in the calculation, namely the minimum energy to which an electron would be followed, so as to agree with the experiment. This procedure consisted of comparing the predicted distribution of track lengths

TABLE III. Factors contributing to detection efficiency.

Effect	Contribution to efficiency for pair of γ's
Mean solid angle	0.45
γ-ray detection (per bank 0.57)	0.32
γ-ray absorption in target, anticounters, etc.	0.77
γ rays not quite anticollinear	0.94
Total	0.10

[13] J. C. Butcher and H. Messel, Nucl. Phys. **20**, 15 (1960).

TABLE IV. Comparison of branching ratio with previous determinations.

Laboratory	Gamma detector	Events minus background	Estimated background	R
CERN (Ref. 7)	NaI and lead glass	52	8±3	$(1.15\pm0.22)\times10^{-8}$
Dubna (Ref. 8)	Total absorption counters	43	7±5	$(1.1\pm0.2)\times10^{-8}$
Berkeley[a]	Lead and counters	5	1±1	$(2.1_{-2.1}^{+1.9})\times10^{-8}$
Columbia (this experiment)	Spark Chambers	36	3±1	$(0.97\pm0.20)\times10^{-8}$

[a] R. B. Bacastow, thesis, University of California Radiation Laboratory Report UCRL-10864 (unpublished); R. B. Bacastow, T. Elioff, R. Larsen, C. Weigand, and T. Ypsilantis, Phys. Rev. Letters 9, 400 (1962).

with the observed distribution produced by γ radiation from stopping π^-

$$\pi^- + p \to \pi^0 + n. \qquad (3)$$
$$\searrow$$
$$2\gamma$$

The results of the efficiency calculation are shown in Fig. 12 where it is seen that for $d=2.0$ radiation lengths, the expected detection efficiency is 61%.

By demanding that an electron travel at least 0.3 radiation lengths (or 2 gaps) in the first 2.0 radiation lengths (≈thickness of a bank of spark chambers), this detection efficiency was reduced to 57%.

To first order, the total detection efficiency for a pair of γ rays is the product of several factors which we list in Table III. In fact, these various effects are coupled. The solid angle varies by almost 2:1 from the beginning of the first chamber to the end of the last. The efficiency for elements close to the edge of a chamber is reduced because only one counter, rather than three, is available to detect the materialized electron. Similarly, the subtraction for premature conversion of the γ rays in the target or elsewhere varies with the direction of the γ rays. We therefore performed the following numerical integration:

$$P'(\gamma)=\int dxdz\frac{\cos\beta}{r^2}\mathrm{eff}_i^2(\beta)\exp[-L(x,z)].$$

The integration is over the plane of the innermost gamma counter (for convenience), β is the angle made with the normal to the spark-chamber plates, $\mathrm{eff}_i(\beta)$ is the efficiency of detection, per γ ray, for different angles of incidence (determined essentially from Fig. 12), $i=1$, 2, or 3 denotes the number of gamma counters available for detection, and L is the path length (expressed in conversion lengths) prior to the first spark chamber.

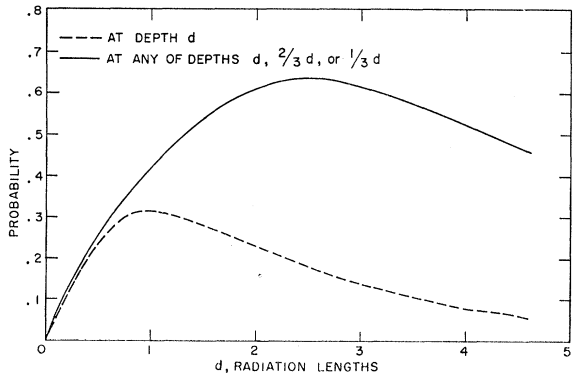

FIG. 12. Monte Carlo calculation of probability of there being one or more electrons at any of depths d, $\frac{2}{3}d$, and $\frac{1}{3}d$ in a shower in stainless steel initiated by a 67.5-MeV γ.

A correction has to be made, however, because the opening angle is not exactly 180°. To first order we may treat this effect separately and define a reduction factor A. Using the Monte Carlo technique to determine A, we find that for a pion stopping in the center of the target, the over-all gamma detection efficiency is

$$P_{\mathrm{center}}(\gamma)=P'(\gamma)A=(0.097)(0.95)=0.092.$$

Finally, we calculate the product of $P'(\gamma)$ and A for 100 points randomly chosen according to the stopping pion distribution and obtain for the total gamma detection efficiency

$$P(\gamma)=0.084\pm0.008,$$

where the error is compounded of an estimated 4% systematic error in the determination of the efficiency for detection of one γ ray (hence 8% in eff^2) and a 5% error in the numerical integration.

C. Small Corrections

We mention briefly three small corrections to the efficiency. First, random electrons form μ decay produced pulses in the eight anticounters and reduced the detection efficiency for events by about 1%. Second, for the first quarter of the run, one γ-γ coincidence ($2A$-$4B$) was improperly set and was only three-fourths efficient. Thus, the efficiency has to be lowered by 1.7%. Last, on the basis of an independent rescan of a 25% sample we take 98%±2% as an estimate of the scanning efficiency. The product of these three factors is

$$P(s)=0.95\pm0.02.$$

D. Summary

The over-all efficiency (per beam particle), is the product of the efficiencies obtained in the last three sections.

$$\mathrm{Eff}/(1\text{-}T)$$
$$=(0.46\pm0.02)(0.084\pm0.008)(0.95\pm0.02)$$
$$=(0.037\pm0.004).$$

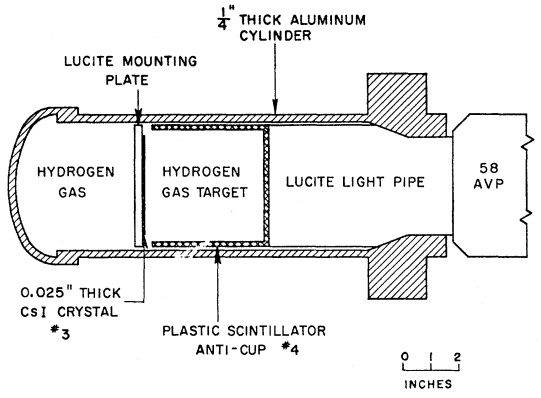

FIG. 13. Diagram of high-pressure gas target. Not shown in figure are counters No. 1 and No. 2 and the absorber which was placed in front of the target.

For comparison with other experiments, we also give the over-all detection efficiency per *stopping pion.*

$$\mathrm{Eff}/(\pi)=\frac{\mathrm{Eff}/(1-T)}{(0.78\pm0.02)}=0.047\pm0.005.$$

V. RESULTS AND COMPARISON WITH PREVIOUS EXPERIMENTS

During the run, we recorded 1.0×10^{11} beam particles. Our experimental value for the branching ratio is then

$$R=\frac{\mathrm{Rate}(\pi^+\rightarrow\pi^0+e^++\nu)}{\mathrm{Rate}(\pi^+\rightarrow\mu^++\nu)}$$

$$=\frac{(\mathrm{events})-(\mathrm{background})}{[\mathrm{Eff}/(1-T)]\times(\mathrm{beam\ particles})}$$

$$=\frac{(39\pm6)-(3\pm1)}{(0.037\pm0.004)(1.00\times10^{11})}$$

$$=(0.97\pm0.20)\times10^{-8}.$$

This result is compared (see Table IV) with previous experimental values obtained using different techniques. In view of the existing discrepancy in the values of $G_V{}^\beta$ and G^μ, it is perhaps appropriate to use the pion beta-decay experiment to define a separate coupling constant $G_V{}^\pi$. On using the formula of Terent'ev,[6] our result implies

$$G_V{}^\pi=(1.37\pm0.15)\times10^{-49}\ \mathrm{erg\ cm^3},$$

in good agreement with the coupling constants derived from nuclear beta decay and muon decay[14]

$$G_V{}^\beta=(1.4029\pm0.0022)\times10^{-49}\ \mathrm{erg\ cm^3},$$
$$G^\mu=(1.4350\pm0.0011)\times10^{-49}\ \mathrm{erg\ cm^3}.$$

[14] As quoted in C. S. Wu, Rev. Mod. Phys. **36**, 618 (1964).

VI. $\pi^-+p\rightarrow\pi^0+n$, A CONFIRMING MEASUREMENT

By exposing the apparatus to π^0 gamma rays (from π^- mesons stopped in hydrogen) we obtained a check on the calculation of the efficiency as well as on the details of the response of the gamma spark chambers.

Negative pions were stopped in the high-pressure hydrogen gas target illustrated in Fig. 13. The active volume of this target was a cylinder whose axis coincided with the beam axis and whose diameter and height were both 4 in. Because of the low density of hydrogen, the thickness of the target, even when it was filled to 100 atm, was only 0.09 g/cm². Since the negative-pion range curve has a full width at half-maximum of 2.4 g/cm² (polyethylene), only about 8% of the pions could stop in the gas. This fraction is more than enough to test the general behavior of the gamma chambers. However, to obtain a reasonable check on the efficiency calculation, it is necessary to know the number of pions stopping in the hydrogen to 5% or better.

Such accuracy was achieved by enclosing the active volume in two different scintillating materials. Preceding the volume was a thin (0.025-in.) CsI crystal. Surrounding the other surfaces was an ⅛-in. thick plastic scintillator cup. A single phototube (58AVP) viewed both scintillators. A pion which stopped in the gas would give only the long (≈1-μsec) CsI pulse, whereas one which penetrated into the anticup would give a short (10-nsec) plastic-scintillator pulse as well. The two types of pulses were distinguished electronically.

Using this arrangement, the stopping pion beam rate $(123\bar{4})$ with the target empty was only three-fifths of the rate with the target filled to 1450 psi of hydrogen. The relevant range curves are shown in Fig. 14, from which we can make a reliable subtraction of the effects with a full target and an empty one, accurate to within 5%.

Spark-chamber pictures were taken with the triggering requirement $(123\bar{4})$ $(\gamma\gamma\bar{A})$. For $(\gamma\gamma)$, we sometimes used the same "half-bank" triggering requirement, $(1A\text{-}3B)+(1B\text{-}3A)+(2A\text{-}4B)+(2B\text{-}4A)$ used in the main run (the four combinations were used either separately or all together). Other pictures were taken with the "full-bank" trigger, (1-3) or (2-4), which does

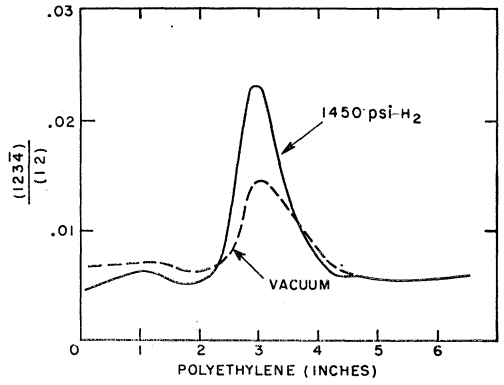

FIG. 14. "Range" curves obtained with the hydrogen target.

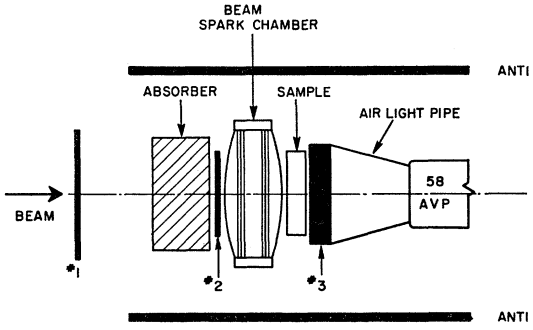

FIG. 15. Beam telescope for hydrogenous samples.

not discriminate so strongly against the large opening angles of gamma rays from reaction (3).

We recorded 800 pictures showing two γ rays. The distributions in three dimensions of the first spark of the conversion electrons agreed with that expected from isotropy of γ production from π^0's. After removing biases owing to solid-angle variation and the opening angle of the gammas, the conversion points were distributed uniformly along the planes of the spark-chamber plates and fell off with depth into the spark-chamber bank in a distance given by the conversion length.

A quantitative check of the γ ray efficiency calculation for the pion beta-decay experiment was made by using the same program to calculate the efficiency for detecting γ rays from reaction (3) and comparing this efficiency with the measured one. For twelve half-hour measurements, we found the experimental detection efficiency

$$P_{\text{expt}}(\gamma)=\frac{(123\bar{4})(\gamma\gamma\bar{A})}{(123\bar{4})_{\text{full}}-(123\bar{4})_{\text{empty}}}(f)-\left(\frac{R+1}{R}\right)\left(\frac{1}{S_{\text{eff}}}\right),$$

where f is the fraction of pictures showing two γ rays, R is the Panofsky ratio, 1.533 ± 0.021, and S_{eff} is the scanning efficiency $(91\pm3\%)$. From measurement to measurement, f varied from 0.48 to 0.58. No subtraction was made for the $(123\bar{4})$ $(\gamma\gamma\bar{A})$ target-empty rate since this rate was only $\approx 1\%$ of the target-full rate.

The efficiencies of the four triggering combinations were found to be equal, within statistics, as were the efficiencies obtained with the three pressures used (250, 900, and 1450 psi). A weighted average of the runs yields

$$P_{\text{expt}}^{1/2}(\gamma)=0.065\pm0.004 \text{ (half-bank triggering, all 4 combinations)}$$

$$P_{\text{expt}}^{1}(\gamma)=0.040\pm0.003 \text{ (full-bank triggering, 1-3 } or \text{ 2-4).}$$

For comparison, the calculated efficiency using the same procedure as was used for the pion beta-decay run (allowing only for the larger opening angles of the gamma rays and the different composition of the target and hence of the self-absorption and stopping distribution)yields

$$P_{\text{calc}}^{1/2}(\gamma)=0.062\pm0.006,$$
$$P_{\text{calc}}^{1}(\gamma)=0.040\pm0.004.$$

The excellent agreement justifies the accuracy claimed for the estimates of spark-chamber γ detection efficiencies.

VII. π^- CAPTURE IN HYDROGENOUS COMPOUNDS

A. Introduction

The fraction (W) of π^- mesons stopping in a hydrogenous material which are captured by hydrogen may be measured by observing the yield of π^0 mesons from the reaction

$$\pi^- + p \to \pi^0 + n,$$
$$\searrow$$
$$2\gamma$$

in an apparatus of known efficiency. Such a measurement has been made at CERN[15] for the compounds LiH, CH_2, and CH and at Dubna[16] for these compounds and $C_4O_2H_8$, H_2O, and TiH as well. The results of CERN are systematically a factor of three higher than those of Dubna. In an effort to resolve this discrepancy, we have measured W for LiH, CH_2, and CH and find results which are consistent only with those of CERN.

B. Experimental Technique

The two gamma rays from the π^0 decay were detected in the same spark chamber and counter array described in Sec. II. The beam telescope, however, was modified to permit the insertion of the samples (see Fig. 15). The spark chambers were triggered on the requirement that the two γ rays $(\gamma\gamma\bar{A})$ occur in coincidence with the stopping beam particle $(12\bar{3}\bar{A})$. For LiH, approximately 30% of these triggers produced pictures having two γ rays. To determine the background, negative pions were stopped in Li and C samples of roughly the same stopping power. Approximately 1000 pictures were taken with each sample.

C. Analysis

The pictures were scanned for two γ rays in opposite banks, using the same criterion (minimum of two sparks in adjacent gaps) that was used in the pion beta-decay experiment. A second scan of 25% of the film showed that the scanning was $(94\pm3)\%$ efficient.

To check that the γ rays observed were really from π^0's produced by π^-'s *stopping* in *hydrogen*, we have plotted in Fig. 16 the distribution in "projected"

[15] M. Chabre, P. Depommier, J. Heintze, and V. Soergel, Phys. Letters 5, 67 (1963).
[16] V. I. Petrukhin and Yu. D. Prokoshkin, Nuovo Cimento 28, 99 (1963).

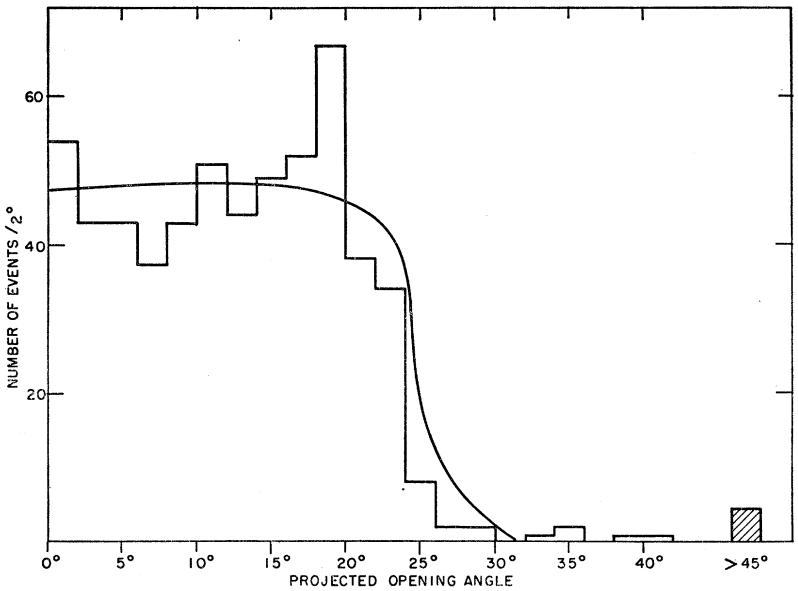

FIG. 16. Histogram of observed distribution in "projected" opening angle of the 600 LiH events. The solid curve is the predicted distribution (using the Monte Carlo technique) for γ's produced by π^- charge exchange at rest on hydrogen.

opening angles of the 600 LiH events. (Note that, as in Sec. III B, the direction of one of the γ rays has been reversed.) The distribution falls abruptly almost to zero at a "projected" angle of 24°, corresponding to the minimum opening angle from π^- capture at rest in hydrogen (156°), indicating that the contribution of charge exchange in flight is unimportant. The background obtained with Li and C samples of the same stopping power was small (3% for LiH, 4% for CH_2, 12% for CH).

Finally, in the analysis all rates were normalized to the entering beam rate (12). The fraction stopping in the sample was obtained by subtracting the $(12\bar{3}\bar{4})$ rate with the sample out from the rate with the sample in. Since the sample was practically completely surrounded by anticounter, particles scattered by the sample would not be confused with stopping particles. A subtraction for stopping electrons ($6\pm3\%$) was made from the range curves. The corresponding muon subtraction was negligible ($\lesssim 2\%$).

D. Results and Discussion

W is obtained from the number of π^0 per π^- stopped by taking into account the Panofsky ratio,[17] 1.533 ± 0.021 and making small corrections for Dalitz pairs. Our results together with those of CERN and Dubna are given in Table V. (Note that in computing W, CERN used a different experimental determination of the Panofsky ratio.)

All of our results are in marked disagreement with those of Dubna and agree very well with those of CERN (except for polyethylene, for which there is a discrepancy of two standard deviations).

[17] V. T. Cocconi, T. Fazzini, G. Fidecaro, M. Legros, N. H. Lipman, and A. W. Merrison, Nuovo Cimento 22, 494 (1961).

Note added in proof. A. F. Dunajtsev and Yu. D. Prokoshkin have recently remeasured the rates of π^- capture in hydrogenous compounds.[17a] They have obtained the following results for W ($\times10^3$)—LiH: 33 ± 4, CH_2: 10.6 ± 1.0, CH: 4.1 ± 0.5, H_2O: 2.6 ± 0.4, $C_4O_2H_8$: 3.3 ± 0.4. We wish to thank Dr. Prokoshkin for communicating these results prior to their publication.

VIII. ABSORPTION IN IMPURE HYDROGEN GAS

From the smallness of the capture rate of π^- mesons in hydrogen nuclei bound in chemical compounds, one might naively expect that even an impurity as small as a few per cent would capture, by π^- transfer, a substantial fraction of the pions stopped in hydrogen gas. Using the gas target described in Sec. VI, we have measured W, the fraction of π^- mesons captured by hydrogen nuclei, in the presence of nitrogen and helium impurities. The results are summarized in Table VI. There is evidently no appreciable transfer of the π^- from hydrogen to a 2% nitrogen impurity. Even for the large helium impurity, the results are consistent with equal molecular capture rates for He and H and little transfer during the cascade from capture to nuclear interaction.

TABLE V. Values of $W\times10^3$. [Numbers in parentheses are π^0/π^- stop]

Target	H_2	LiH	CH_2	CH
This experiment	1030 ± 110 (615 ± 70)	40 ± 4 (24 ± 3)	17.9 ± 1.9 (10.7 ± 1.1)	5.5 ± 0.7 (3.3 ± 0.4)
CERN (Ref. 5)	974 ± 79 (594 ± 48)	39 ± 3 (24 ± 2)	13.9 ± 1.1 (8.5 ± 0.7)	5.4 ± 0.5 (3.3 ± 0.3)
Dubna (Ref. 6)	···	13.9 ± 1.5	4.4 ± 0.4	1.7 ± 0.2

[17a] Nuovo Cimento (to be published).

TABLE VI. Values of W in different gas mixtures.

	H_2-N_2	H_2-He-N_2
H_2 partial pressure	1400 psi	900 psi
N_2 partial pressure	30 psi	10 psi
He partial pressure	...	400 psi
Two γ events	57	28
W	0.97±0.15	0.50±0.23

ACKNOWLEDGMENTS

The experiment could not have been done without the continual assistance of the entire Nevis staff. We gratefully acknowledge the special contributions of R. Barbee who assembled the spark chambers and gave technical help throughout the experiment, of J. Shill and L. Todor who assisted with mechanical design, and of J. Reilly and S. Stein who constructed the equipment. The electronics, designed by W. LeCroy, gave trouble-free performance. P. Nemethy kindly assisted us during the extended operation of the experiment. Finally, we are particularly grateful to Miss Ann Therrien and A. Kenny who carefully scanned the film, and to Mrs. Anna McDowell who painstakingly drew the figures.

PHYSICAL REVIEW VOLUME 136, NUMBER 5B 7 DECEMBER 1964

Determination of the τ^+ Branching Ratio*

ANDREW CALLAHAN, ROBERT MARCH, AND ROBERT STARK
Department of Physics, University of Wisconsin, Madison, Wisconsin
(Received 6 July 1964)

The branching ratio for the τ^+ decay mode ($K^+ \to \pi^+\pi^+\pi^-$) has been obtained from 2332 τ^+ decays in a bubble chamber containing C_3F_8. We find that (5.54±0.12)% of all K^+ decay by this mode. Combining this result with four previous measurements gives a weighted "world mean" of (5.46±0.09)%.

INTRODUCTION

THE τ decay mode of charged K mesons ($K^\pm \to \pi^\pm + \pi^+ + \pi^-$) is easily recognized in most visual detectors. For this reason its branching ratio is widely used as a calibration of total K flux in measurements of cross sections and other K-decay mode branching ratios. Because of unresolved discrepancies in previous measurements[1–5] of the τ^+ branching ratio, we have undertaken a new measurement of substantially higher statistical accuracy.

The measurement was performed with K^+ in a separated beam from the bevatron, brought to rest in the Lawrence Radiation Laboratory 30-in. heavy-liquid bubble chamber. The chamber contained C_3F_8 at a density of 1.22 g/cm², radiation length 28 cm. In this liquid, no τ^+ decay secondary from a K^+ at rest has a range of over 8.8 cm, and at least two secondaries stop in the chamber in every τ^+ decay.

SCANNING

The scanning was done by the three authors. An along-the-track scan was used, following each K from where it entered a chosen fiducial volume until it either decayed or left the volume. Events were classified as to whether they decayed in flight or at rest as determined by visual analysis of the K^+ ionization. Cases where the K^+ had undergone a nuclear interaction (projected angle of scatter greater than 15°) before decay were recorded separately. These categories were chosen as a check on the result, in anticipation of difficulties due to π contamination of the beam; they are combined in the final quoted rate. The results are shown in Table I.

It is necessary to include both decays at rest and in flight in the sample of data because τ decays in flight are usually kinematically obvious, while only ionization information is available for most of the other

TABLE I. Results of scanning.

τ decays		Other K^+ decays	
Rest	1765	Rest	30 818
Flight	195	Flight	2274
Interaction[a]	372	Interaction[a]	5982
	2332	Ambiguous	179
			39 253

[a] K undergoes nuclear scattering before stopping.

* Work supported in part by the U. S. Atomic Energy Commission Contract No. AT(11-1)-881.

[1] R. W. Birge, D. H. Perkins, J. R. Peterson, D. H. Stork, and M. N. Whitehead, Nuovo Cimento 4, 834 (1956).
[2] G. Alexander, R. H. W. Johnston, and C. O'Ceallaigh, Nuovo Cimento 6, 478 (1957).
[3] S. Taylor, G. Harris, J. Orear, J. Lee, and P. Baumel, Phys. Rev. 114, 359 (1959).
[4] B. P. Roe, D. Sinclair, J. L. Brown, D. A. Glaser, J. A. Kadyk, and G. H. Trilling, Phys. Rev. Letters 7, 346 (1961).
[5] F. S. Shaklee, thesis, University of Michigan Technical Report 4938-2-T, 1964 (unpublished).